# Mutagenesis of Glycine 179 Modulates Both Catalytic Efficiency and Reduced Pyridine Nucleotide Specificity in Cytochrome $b_5$ Reductase†

Glenn W. Roma, Louis J. Crowley, C. Ainsley Davis, and Michael J. Barber*

*Department of Biochemistry and Molecular Biology, College of Medicine and the H. Lee Moffitt Cancer Center and Research Institute, University of South Florida, Tampa, Florida 33612*

*Received June 16, 2005; Revised Manuscript Received August 3, 2005*

ABSTRACT: Cytochrome $b_5$ reductase (c$b_5$r), a member of the ferredoxin:NADP$^+$ reductase family of flavoprotein transhydrogenases, catalyzes the NADH-dependent reduction of cytochrome $b_5$. Within this family, a conserved "GxGxxP" sequence motif has been implicated in binding reduced pyridine nucleotides. However, Glycine 179, a conserved residue in c$b_5$r primary structures, precedes this six-residue "$^{180}$GxGxxP$^{185}$" motif that has been identified as binding the adenosine moiety of NADH. To investigate the role of G179 in NADH complex formation and NAD(P)H specificity, a series of rat c$b_5$r variants were generated, corresponding to G179A, G179P, G179T, and G179V, recombinantly expressed in *Escherichia coli* and purified to homogeneity. Each mutant protein was found to incorporate FAD in a 1:1 cofactor/protein stoichiometry and exhibited absorption and CD spectra that were identical to those of wild-type c$b_5$r, indicating both correct protein folding and similar flavin environments, while oxidation−reduction potentials for the FAD/FADH$_2$ couple ($n = 2$) were also comparable to the wild-type protein ($E^{\circ\prime} = -272$ mV). All four mutants showed decreased NADH:ferricyanide reductase activities, with $k_{cat}$ decreasing in the order WT > G179A > G179P > G179T > G179V, with the G179V variant retaining only 1.5% of the wild-type activity. The affinity for NADH also decreased in the order WT > G179A > G179P > G179T > G179V, with the $K_m^{NADH}$ for G179V 180-fold greater than that of the wild type. Both $K_s^{H_4NAD}$ and $K_s^{NAD^+}$ values confirmed that the G179 mutants had both compromised NADH- and NAD$^+$-binding affinities. Determination of the NADH/NADPH specificity constant for the various mutants indicated that G179 also participated in pyridine nucleotide selectivity, with the G179V variant preferring NADPH approximately 8000 times more than wild-type c$b_5$r. These results demonstrated that, while G179 was not critical for either flavin incorporation or maintenance of the appropriate flavin environment in c$b_5$r, G179 was required for both effective NADH/NADPH selectivity and to maintain the correct orientation and position of the conserved cysteine in the proline-rich "CGpppM" motif that is critical for optimum NADH binding and efficient hydride transfer.

Cytochrome $b_5$ reductase (c$b_5$r,[1] EC 1.6.2.2)[2] catalyzes the single-electron reduction of ferricytochrome $b_5$ to ferrocytochrome $b_5$ using the reduced pyridine nucleotide coenzyme, NADH, as the physiological electron donor. The rate-limiting step in catalysis has been identified as a hydride ion transfer step involving the donation of one proton and two electrons from the nicotinamide moiety of NADH to the oxidized FAD prosthetic group of c$b_5$r (*1*). In mammalian species, microsomal and cytosolic c$b_5$r isozymes provide reducing equivalents for a variety of physiologically important metabolic processes that include methemoglobin reduction (*2*, *3*), fatty acid elongation and desaturation (*4*), cholesterol biosynthesis (*5*), and the cytochrome P450-mediated hydroxylations of steroid hormones and xenobiotics (*6*), such as the reaction catalyzed by cytochrome P450 3A4 (*7*) and the reduction of *N*-hydroxylamine (*8*).

Cytochrome $b_5$ reductase sequences have been identified within the genomes of a diverse array of eukaryotic organisms that include fungi [*Mortierella alpina* (*9*)], yeast [*Saccharomyces cerevisiae* (*10*)], plants [*Arabidopsis thaliana* (*11*)], nematodes [*Caenorhabditis elegans* (*12*)], insects [*Drosophila melanogaster* (*13*)], fish [*Danio rerio* (*14*)], amphibians [*Xenopus laevis* (*15*)], birds [*Gallus gallus* (*16*)], and mammals [*Rattus norvegicus* (*17*)]. Multiple sequence alignments have revealed extensive primary structure conservation within c$b_5$r homologues with the most diverse sequences [*Homo sapiens* (*18*) and *Plasmodium yoelii* (*19*)] retaining approximately 25% sequence identity.

† This work was supported by Grants GM 32696 from the National Institutes of Health (to M.J.B.) and 9701708 and 9910034V from the American Heart Association, Florida/Puerto Rico Affiliate (to M.J.B.).

* To whom correspondence should be addressed: Department of Biochemistry and Molecular Biology, University of South Florida, College of Medicine, 12901 Bruce B. Downs Blvd., MDC 007, Tampa, FL 33612. Telephone: (813) 974-9702. Fax: (813) 974-7357. E-mail mbarber@hsc.usf.edu.

[1] Abbreviations: c$b_5$r, cytochrome $b_5$ reductase; c$b_5$, cytochrome $b_5$; CD, circular dichroism; FNR, ferredoxin:NADP$^+$ reductase; FPLC, fast protein liquid chromatography; NADH:FR, NADH:ferricyanide reductase; NADH:BR, NADH:cytochrome $b_5$ reductase; $H_4$NAD, 1,4,5,6-tetrahydro-NAD; IPTG, isopropyl-$\beta$-D-thioglucopyranoside; PAGE, polyacrylamide gel electrophoresis; PMSF, phenylmethylsulfonyl fluoride; SDS, sodium dodecyl sulfate; SHE, standard hydrogen electrode; $\mu$, ionic strength.

[2] Amino acid residues are numbered with respect to their position in the sequence of the full-length, membrane-binding form of c$b_5$r (GenBank accession number P20070).

10.1021/bi051165t CCC: $30.25 
Published on Web 09/23/2005

**A**

| Species | Sequence | Accession # |
|---|---|---|
| *H. sapiens* | $^{173}$SVGMIA**G**GTGITPMLQVIRAI$^{193}$ | NP_000389 |
| *B. taurus* | $^{173}$SVGMIA**G**GTGITPMLQVIRAI$^{193}$ | P07514 |
| *S. scrofa* | $^{145}$SVGMIA**G**GTGITPMLQVIRAI$^{163}$ | 1NDH |
| *R. norvegicus* | $^{173}$SVGMIA**G**GTGITPMLQVIRAV$^{193}$ | P20070 |
| *M. musculus* | $^{176}$KLGMIA**G**GTGITPMLQLIRAI$^{197}$ | NP_084063 |
| *G. gallus* | $^{127}$HLGMIA**G**GTGITPMLQLIRHI$^{147}$ | XP_416445 |
| *D. rerio* | $^{176}$SLGLIA**G**GTGITPMLQLIRDI$^{196}$ | AAH45880 |
| *I. furcatus* | $^{173}$HLGMIA**G**GTGITPMLQIIRGI$^{193}$ | CK408748 |
| *X. laevis* | $^{173}$HLGMIA**G**GTGITPMLQLIRAI$^{193}$ | BC045265 |
| *D. melanogaster* | $^{184}$RVNMIA**G**GTGITPMLQLAREV$^{204}$ | NM_168479 |
| *A. gambiae* | $^{229}$QVGLIA**G**GTGITPMLQLIREV$^{249}$ | XM_309347 |
| *C. elegans* | $^{182}$HLSMIA**G**GTGITPMLQVIAAI$^{202}$ | NP_504638 |
| *S. japonicum* | $^{177}$RVNMIC**G**GSGITPMFQLLSYI$^{197}$ | AAP05890 |
| *A. thaliana* | $^{155}$AFGMLA**G**GSGITPMFQVARAI$^{175}$ | T52470 |
| *C. maxima* | $^{189}$HIGMIA**G**GTGITPMLQVIDAI$^{209}$ | AAK69398 |
| *Z. mays* | $^{153}$AFGMLA**G**GSGITPMFQVARAI$^{173}$ | AAD17694 |
| *O. sativa* | $^{179}$QIGMIA**G**GTGITPMLQVVRAI$^{199}$ | AK071324 |
| *M. acuminata* | $^{38}$DIGMIA**G**GTGITPMLQVIKAI$^{58}$ | AAR88781 |
| *S. pombe* | $^{168}$HFGMIA**G**GTGITPMLQIIRAV$^{188}$ | NP_587852 |
| *N. crassa* | $^{175}$HFGMVA**G**GTGITPMLQVIRAI$^{195}$ | XP_322302 |
| *M. alpina* | $^{165}$AIGMIA**G**GTGLTPMLQIIRAI$^{185}$ | AB020034 |
| *L. major* | $^{167}$AYAAIA**G**GTGITPILQIIHAI$^{187}$ | CAB92390 |
| *G. zeae* | $^{142}$KIGLIA**G**GTGITPMFQVIRAV$^{162}$ | BAC66099 |
| *D. discoideum* | $^{161}$SIGMLA**G**GTGITPMLQVIKAI$^{181}$ | EAL64774 |
| *P. falciparum* | $^{220}$HIVMIA**G**GTGMTPFFRLINHL$^{240}$ | CAD52795 |
| *S. cerevisiae* | $^{186}$HLGMIA**G**GTGIAPMYQIMKAI$^{206}$ | CAA86908 |
| *S. cerevisiaeOM* | $^{161}$SITLLG**A**GTGINPLYQLAHHI$^{181}$ | P36060 |
| | :: :*:*::*: :: | |

**B**


**C**

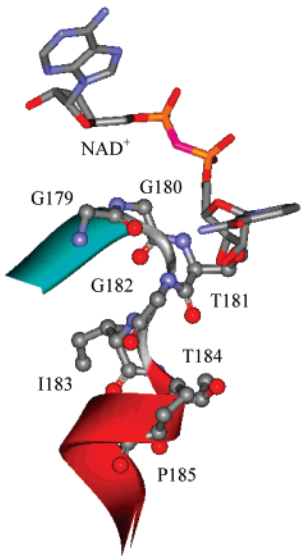


FIGURE 1: Multiple sequence alignment of c$b_5$r primary structures. (A) Various eukaryotic c$b_5$r amino acid sequences deposited in GenBank were retrieved and aligned using the CLUSTAL X algorithm (*46*), and the alignment was optimized for maximum sequence conservation. Only the portions of the sequences surrounding the conserved pyridine nucleotide-binding "GxGxxP" motif are shown for clarity. Beginning and ending residue numbers within the translated GenBank sequences are indicated by superscripts, while the conserved glycine residue corresponding to G179 in *R. norvegicus* c$b_5$r is shown in bold and underlined. The consensus sequence is also shown below with identical residues indicated by "*" and similar residues indicated by ":". *S. cerevisiae* OM corresponds to the sequence of the outer mitochondrial form of *S. cerevisiae* c$b_5$r (*24*). (B) Graphical representation (sequence logo) of the amino acid residues present at positions 176−188 in the primary sequences of 50 c$b_5$r sequences deposited in GenBank. The logo consists of stacks of symbols (one stack for each position in the sequence), with the overall height of the stack indicating the sequence conservation at that position and the height of the symbols within the stack indicating the relative frequency of each amino acid at that position (*47*). (C) Schematic diagram of a portion of the *R. norvegicus* c$b_5$r X-ray crystal structure (PDB code 1IB0) showing the arrangements of the amino acids that comprise the conserved "GxGxxP" motif and residue G179 that precedes the motif. Amino acid residues are shown in "ball-and-stick" representation using the CPK color scheme, while the appropriate portion of the peptide backbone is displayed as a ribbon diagram. The location of the complexed $NAD^+$ is shown in "stick" representation using the CPK color scheme.

Structural studies of a soluble form of recombinant rat c$b_5$r have shown the enzyme to be composed of an amino-terminal FAD-binding lobe that comprises residues I33−G143 and a carboxyl-terminal NADH-binding lobe that comprises residues V171−F300, linked by a short three-stranded antiparallel ***β***-sheet "hinge" region (residues P144−T170) that is required to correctly orient the FAD- and NADH-binding lobes for efficient intramolecular electron transfer (*20*).

Within the c$b_5$r primary structure, four sequence motifs have been identified that are involved in either flavin binding ("$RxY^{T}_{S}xx^{S}_{N}$") and FAD specificity ("$Gxx^{S}_{T}$") or reduced pyridine nucleotide binding ("GxGxxP" and "CGxxxxM") (*21*, *22*), together with several residues that have been shown to regulate NADH/NADPH selectivity (*23*). One of these conserved motifs involved in pyridine nucleotide binding corresponds to the six amino acid residue motif, "GxGxxP", that comprises residues G180−P185 in the carboxyl-terminal lobe of rat c$b_5$r (Figure 1). However, structural studies have identified a number of additional residues that also surround this motif in the primary sequence and that are potentially involved in regulating nucleotide binding, including G179, which is obligatorily conserved in all c$b_5$r primary structures identified to date, with the exception of the outer mitochondrial membrane form of *S. cerevisiae* c$b_5$r (*24*).

Within the X-ray structure of the rat c$b_5$r diaphorase domain (PDB code 1I7P), G179 has been shown to be located at the terminus of the strand N$\beta$1, which is part of a six-stranded parallel $\beta$-sheet motif, and just prior to the start of the 16-residue helical segment N$\alpha$1, which comprises residues G180−K195, both of which comprise part of the pyridine nucleotide-binding lobe (*20*). Residues G179−G182 form a compact four residue segment of the sequence that effectively reverses the direction of the polypeptide backbone and initiates the start of the $\alpha$-helical segment. In addition, analysis of the diaphorase domain structure obtained in complex with $NAD^+$ (PDB code 1IB0) has revealed that, while G179 provides no direct electrostatic or hydrogen-bond contacts with either the nicotinamide or ribose moieties of the bound $NAD^+$, the two conserved glycine residues in the adjacent "GxGxxP" motif, corresponding to G180 and G182, do participate in hydrophobic contacts with the AMP portion of the pyridine nucleotide substrate (Figure 1C).

The "GxGxxP" pyridine nucleotide-binding motif is conserved in all other members of the ferredoxin:$NADP^+$ reductase superfamily of flavoprotein transhydrogenases,

Table 1: Mutagenic Oligonucleotide Primers Used in the Generation of the Different G179 c$b_5$r Variants

| variant | primer sequence (5′ → 3′)[a] | restriction site |
|---|---|---|
| G179A | 5′-GTA-GGC-ATG-ATT-GCA-G**C*T***-GGG-ACA-GGC-ATC-ACC-CCA-3′ | +*Pvu*II |
| G179P | 5′-GTA-GGC-ATG-ATT-GC***T*-CC**A-GGG-ACA-GGC-ATC-ACC-CCA-3′ | +*Bpm*I |
| G179T | 5′-GTA-GGC-ATG-ATT-GCA-***ACC***-GGG-ACA-GGC-ATC-ACC-CCA-3′ | +*Nci*I |
| G179V | 5′-GTA-GGC-ATG-ATT-GC***C***-G**TG**-GGG-ACA-GGC-ATC-ACC-CCA-3′ | +*Dsa*I |
| wild type | 5′-GTA-GGC-ATG-ATT-GCA-GGA-GGG-ACA-GGC-ATC-ACC-CCA-3′ | |
| amino acid | N- V G M I A G G T G I T P -C | |

[a] Nucleotides shown in bold encode the mutated residue. Silent mutations, shown in italics, resulted in the elimination (−) or addition (+) of the indicated restriction site.

including the prototypical member, ferredoxin:$NADP^+$ reductase (FNR) (*21*). However, the nature of the residue preceding the motif exhibits some heterogeneity, although amino acids with primarily hydrophobic side chains appear to comprise the most frequently utilized residues. Further, studies of the determinants of coenzyme specificity in *Anabaena* PCC7119 FNR have indicated that amino acid residues that are not directly situated in the 2′-phosphate $NADP^+$-interacting region, such as T155 (which is equivalent to G179 in c$b_5$r), may influence $NADP^+/NAD^+$ selectivity (*25*).

To probe the role of G179 in c$b_5$r structure and function, we have utilized site-directed mutagenesis as a tool to replace the conserved glycine residue at position 179 in the rat c$b_5$r diaphorase domain with the corresponding amino acid residues (A, P, T, and V) that have been shown to commonly occur at the equivalent positions within other members of the FNR superfamily to primarily examine the effects of these substitutions on the spectroscopic and thermodynamic properties of the FAD prosthetic group and interactions with the physiological reducing substrate, NADH.

## EXPERIMENTAL PROCEDURES

*Materials.* NADH, NADPH, $NAD^+$, riboflavin, phenylmethylsulfonyl fluoride (PMSF), and Tris base were purchased from Sigma Chemical Co. (St. Louis, MO). MOPS was purchased from Calbiochem (San Diego, CA). *Pfu* Turbo polymerases and Epicurian *Escherichia coli* BL21 (DE3)-RIL cells were obtained from Stratagene (La Jolla, CA). Restriction enzymes including *Bpm*I and *Dsa*I were obtained from New England Biolabs (Beverley, MA), and the pET23b expression vector was obtained from Novagen (Madison, WI). Oligonucleotide primers were obtained from IDT (Coralville, IA). Isopropyl-$\beta$-D-thioglucopyranoside (IPTG) was obtained from Research Products Intl. (Mt. Prospect, IL), while Tryptone and yeast extract were obtained from EM Science (Gibbstown, NJ). Reagents for plasmid preparation and agarose gel extraction were purchased from Qiagen, Inc. (Valencia, CA). 1,4,5,6-Tetrahydro-NAD ($H_4$NAD) was synthesized as described by Murataliev et al. (*26*). Nucleotide sequencing was performed by the Molecular Biology Core Facility of the H. Lee Moffitt Cancer Center and Research Institute at the University of South Florida.

*Site-Directed Mutagenesis, Protein Expression, and Purification.* Site-directed mutagenesis of the pH4CB5R construct was performed as previously described (*27*) using the oligonucleotide primers and their complements shown in Table 1 that effected the required codon change and either deleted or inserted a silent restriction site that facilitated subsequent mutant screening. Thus, for the G179A variant, the primers affected both the alanine substitution and added a *Pvu*II restriction site. Positively screened constructs were then used to transform competent *E. coli* BL21 (DE3)-RIL cells, and the resulting c$b_5$r variants were purified to homogeneity as previously described using NTA-agarose affinity and gel-filtration chromatographies (*27*). Sodium dodecyl sulfate−polyacrylamide gel electrophoresis (SDS−PAGE) analyses were performed as described by Laemmli (*28*), while recombinant soluble rat cytochrome $b_5$ was isolated as described by Beck-von Bodman et al. (*29*).

*Spectroscopy.* UV/vis spectra for the various c$b_5$r mutants were obtained using a HP (Agilent Technologies, Palo Alto, CA) 8453 diode-array spectrophotometer. Concentrations of native c$b_5$r and the G179 variants were estimated using $A_{340} = 10.6\ cm^{-1}\ mM^{-1}$ (*27*). UV and visible circular dichroism (CD) spectra were obtained using a JASCO (Easton, MD) J710 spectropolarimeter in 10 mM phosphate buffer as described previously (*27*). Fluorescence spectra were obtained using a Shimadzu (Columbia, MD) RF-2501PC spectrofluorophotometer as previously described (*27*). Spectroscopic titrations of either $H_4$NAD or $NAD^+$ binding to wild-type c$b_5$r and the selected mutants were performed at 23 °C using matched, two-compartment cuvettes with individual chamber path lengths of 0.439 cm as described by Barber et al. (*30*). Absorbance changes were plotted versus the nucleotide concentration, and a simple hyperbolic equation was used to fit the data and to determine the spectral binding constants ($K_s$).

*Initial-Rate Enzyme Kinetics.* All activity assays were performed in triplicate and were routinely determined at 25 °C in 116 mM MOPS buffer ($\mu = 0.05$), containing 0.1 mM EDTA at pH 7.0. NADH:ferricyanide reductase (NADH:FR) activities were determined at 340 nm as previously described (*27*). NADH:cytochrome $b_5$ reductase (NADH:BR) activities were determined at 423 nm in the presence of 200 $\mu$M NADH and 0.5−50 $\mu$M cytochrome $b_5$. Enzyme activities are expressed in terms of $\mu$mol of NADH consumed $min^{-1}$ (nmol of FAD)$^{-1}$. Initial-rate data were analyzed using the software "Enzfit" (Elsevier Biosoft, Ferguson, MO) to yield individual values for the apparent $k_{cat}$ and $K_m$.

*Thermostability Measurements.* Thermal stability profiles for both the wild-type and mutant proteins were determined by monitoring both the release of the FAD prosthetic group, indicated by the increase in intrinsic flavin fluorescence, and the loss of NADH:FR activity as previously described (*27*). NADH:FR activities were assayed for all samples immediately following both dilution and at the conclusion of the inactivation profile, and the average of these values were plotted relative to the initial enzyme activity at 0 °C.

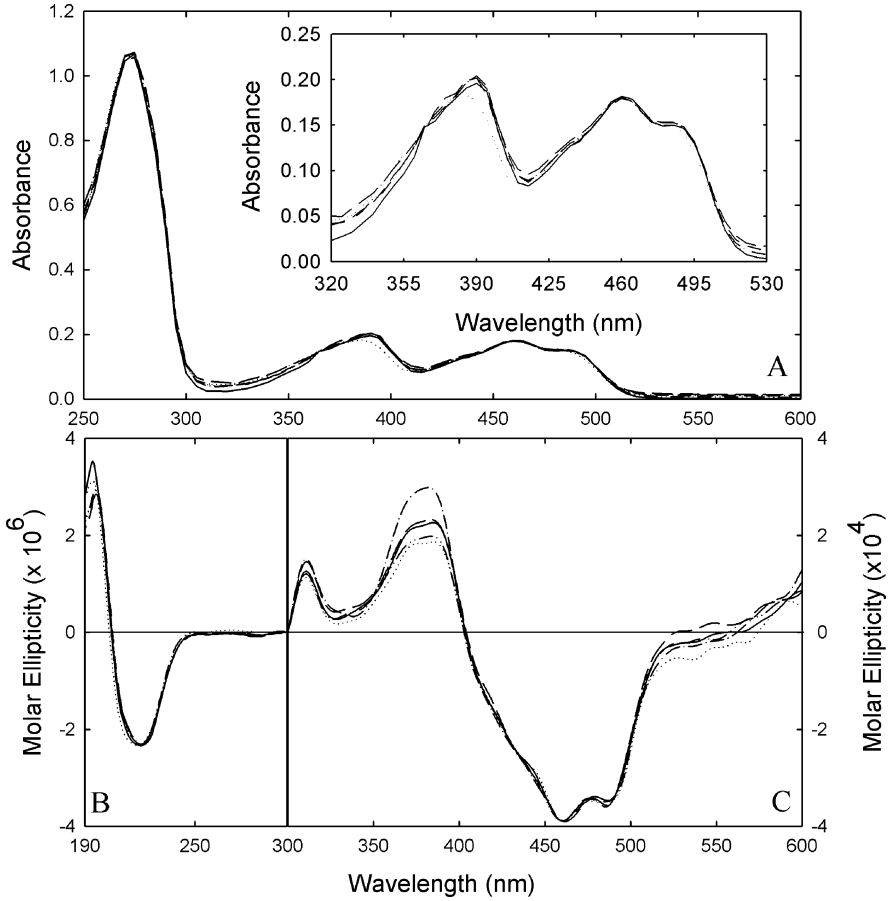


FIGURE 2: UV/vis absorption and CD spectra of c$b_5$r and the various G179 mutants. (A) UV/vis absorption spectra were obtained for oxidized samples of c$b_5$r and the various G179 mutants at equivalent flavin concentrations (1.7 $\mu$M FAD) in 10 mM phosphate buffer, containing 0.1 mM EDTA at pH 7.0. The inset shows an expanded region of the visible spectrum where the flavin prosthetic group makes a major contribution. Individual spectra correspond to wild-type c$b_5$r (—), G179A (- - -), G179P (···), G179T (-·-), and G179V (-··-). (B) UV CD spectra were recorded using enzyme samples (7 $\mu$M FAD) in 10 mM phosphate buffer, containing 0.1 mM EDTA at pH 7.0. (C) Visible CD spectra were recorded using enzyme samples (50 $\mu$M FAD) in 10 mM phosphate buffer, containing 0.1 mM EDTA at pH 7.0. Line styles shown in B and C are the same as those depicted in A.

*Potentiometry and Charge-Transfer Complex Determination.* Oxidation−reduction midpoint potentials for the flavin prosthetic group were determined utilizing the dye equilibration method as described by Massey (*31*) and Marohnic et al. (*23*) using phenosafranine ($E^{o\prime} = -252$ mV) as an indicator. Standard midpoint potentials ($E^{o\prime}$, $n = 2$) for the FAD/$FADH_2$ redox couple were calculated from the plot of $\log([\text{oxidized}]/[\text{reduced}])_{FAD}$ versus the potential, as indicated by the dye. Redox potentials are referenced to the standard hydrogen electrode (SHE) and are considered accurate to ±5 mV. Charge-transfer complex formation was monitored in the near-IR wavelength range of 600−1000 nm during redox titrations performed in the presence of $NAD^+$ (2 mM).

## RESULTS

*Mutagenesis, Expression, and Protein Purification.* Mutant constructs encoding the four different c$b_5$r variants, G179A, P, T, and V, which corresponded to the most frequently encountered amino acid residues occurring at positions corresponding to G179 in the FNR superfamily of pyridine nucleotide-dependent flavoprotein transhydrogenases, were generated through directed mutagenesis of the original four-histidine tagged c$b_5$r construct. Nucleotide sequencing confirmed the fidelity of each construct, and each of the mutant proteins was subsequently expressed in the *E. coli* strain BL21(DE3)-RIL and purified to homogeneity by Ni-chelate chromatography and gel-filtration fast protein liquid chromatography (FPLC). Evaluation of the expression yields of the various mutants indicated that all four G179 variants were expressed at levels comparable to that of the wild-type domain. All four mutants were purified to apparent homogeneity as evident by the presence of single-protein bands following SDS−PAGE analysis of the various mutants, which also indicated molecular masses comparable to that of the native enzyme ($M_r$, approximately 32 kDa).

*Spectroscopy.* The oxidized forms of all four purified G179 variants were yellow in color, indicating the incorporation of a flavin prosthetic group and confirming that G179 did not provide backbone or side-chain contacts that were essential for the stable incorporation of the flavin prosthetic group into any of the c$b_5$r variants.

UV/vis absorbance spectra were obtained for oxidized samples of each mutant and wild-type c$b_5$r and are compared in Figure 2A. The G179A, G179P, G179T, and G179V variants each exhibited spectra comparable to that of the wild-type enzyme with an aromatic absorption maximum detected at 270 nm in the UV region of the spectrum and a peak at 461 nm with a associated pronounced shoulder in the range of 485−500 nm in the visible region of the spectrum, attributable to protein-bound flavin. None of the

Table 2: NAD(P)H:FR and NADH:BR Kinetic Constants Obtained for the Various c$b_5$r G179 Mutants

| | NADH:FR activity | | | | NADH:BR activity | | NADPH:FR activity | | | nucleotide specificity constant |
|---|---|---|---|---|---|---|---|---|---|---|
| protein | $k_{cat}$ ($s^{-1}$) | $K_m^{NADH}$ ($\mu$M) | $K_m^{Fe(CN)_6}$ ($\mu$M) | $k_{cat}/K_m^{NADH}$ ($s^{-1}$ $M^{-1}$) | $k_{cat}$ ($s^{-1}$) | $K_m^{cyt\ b}$ ($\mu$M) | $k_{cat}$ ($s^{-1}$) | $K_m^{NADPH}$ ($\mu$M) | $k_{cat}/K_m^{NADPH}$ ($s^{-1}$ $M^{-1}$) | $\Delta$[a] |
| G179A | $559 \pm 18$ | $25 \pm 2$ | $8 \pm 1$ | $2.3 \pm 0.2 \times 10^7$ | $245 \pm 17$ | $8 \pm 1$ | $48 \pm 8$ | $1360 \pm 322$ | $3.9 \pm 2 \times 10^4$ | $1.7 \times 10^{-3}$ |
| G179P | $42 \pm 2$ | $595 \pm 40$ | $7 \pm 1$ | $7.1 \pm 0.8 \times 10^4$ | $10 \pm 1$ | $1 \pm 1$ | $17 \pm 3$ | $2317 \pm 702$ | $8.4 \pm 4 \times 10^3$ | $1.2 \times 10^{-1}$ |
| G179T | $33 \pm 2$ | $662 \pm 37$ | $8 \pm 1$ | $5.1 \pm 0.5 \times 10^4$ | $18 \pm 2$ | $43 \pm 2$ | $12 \pm 2$ | $507 \pm 145$ | $2.6 \pm 1 \times 10^4$ | $5.1 \times 10^{-1}$ |
| G179V | $12 \pm 1$ | $1077 \pm 78$ | $7 \pm 1$ | $1.1 \pm 0.2 \times 10^4$ | $17 \pm 2$ | $107 \pm 8$ | $8 \pm 1$ | $375 \pm 25$ | $2.2 \pm 1 \times 10^4$ | $1.9 \times 10^0$ |
| wild type | $800 \pm 17$ | $6 \pm 1$ | $8 \pm 1$ | $1.4 \pm 0.3 \times 10^8$ | $400 \pm 17$ | $13 \pm 1$ | $33 \pm 5$ | $924 \pm 46$ | $3.6 \pm 2 \times 10^4$ | $2.6 \times 10^{-4}$ |

[a] The nucleotide specificity constant, $\Delta$, is defined as the ratio $\{(k_{cat}/K_m^{NADPH})/(k_{cat}/K_m^{NADH})\}$.

mutant visible spectra was blue-shifted with respect that of the wild-type protein, as has been previously demonstrated for mutations of other residues, such as R91P (*27*) and Y93H (*32*), suggesting that none of the G179 substitutions had any significant influence on the spectroscopic properties of the FAD. Blue shifts in the visible absorbance spectra of flavoproteins have previously been attributed to changes in the hydrophilicity of the flavin environment near the N(5) locus of the isoalloxazine ring (*33*, *34*). Absorbance ratios ($A_{280\ nm/461\ nm}$) were within the range $6.1 \pm 0.2$ for all four mutants and were comparable to that obtained for wild-type c$b_5$r, indicating a full complement of the FAD prosthetic group.

To assess the secondary structural content of each of the mutant enzymes, CD spectra were recorded in the UV wavelength range (190−300 nm). As shown in Figure 2B, all of the c$b_5$r variants exhibited positive CD from 190 to 210 nm and negative CD from 210 to 250 nm, with all of the spectra retaining both positive and negative intensities very similar to that of the wild-type domain. The absence of any significant differences between the spectra of the wild-type and mutant proteins suggested conservation of the secondary-structure architecture and that none of the G179 residue substitutions had any deleterious effects on the folding of the diaphorase domain.

Visible CD spectroscopy was utilized to examine the environment of the FAD prosthetic group. As shown in Figure 2C, all four mutants exhibited visible CD spectra that were virtually indistinguishable from that of the wild-type domain and indicated that none of the amino acid substitutions had any significant effect on the conformation of the bound chromophore. Previous spectroscopic analyses of c$b_5$r mutants containing altered residues that are involved in FAD binding, such as S127 (*35*), have revealed visible CD to be a sensitive indicator of flavin conformation changes.

The extent of quenching of the intrinsic fluorescence because of the FAD prosthetic group of c$b_5$r has also proven to be a sensitive indicator of the retention of the native flavin environment. To probe the flavin fluorescence quenching of the various G179 mutants, both excitation and emission fluorescence spectra were recorded prior to and following heat denaturation of the various mutants. Prior to denaturation, wild-type c$b_5$r and the G179 variants quenched the flavin fluorescence to varying degrees ranging from 95% for the wild-type enzyme to only 60% for the G179V variant, with the G179A, P, and T variants being quenched 89, 81, and 68%, respectively.

*Thermal Stability.* To examine the influence of the various G179 residue substitutions on the stabilities of the resulting proteins, thermal denaturation profiles were generated for wild-type c$b_5$r and each of the mutant proteins by measuring both changes in the intrinsic flavin fluorescence emission intensity ($\lambda_{em} = 523$ nm) and retention of NADH:FR activity following incubation of the proteins at temperatures ranging from 0 to 100 °C. Changes in the intrinsic fluorescence of the cofactor or the retention of NADH:FR activity following thermal denaturation was an effective indicator of the stability of the core structure of the protein. $T_{50}$ values (the temperature at which 50% of maximum fluorescence or 50% retention of NADH:FR activity was detected) increased in the order G179A < G179P < G179T < WT < G179V, with all variants exhibiting $T_{50}$ values in the range between 52 and 57 °C, which suggested that none of the substitutions had a dramatic effect on the thermal stability of flavin binding. The G179T variant exhibited a $T_{50}$ value of approximately 54 °C, in good agreement with the value of 55 °C obtained for wild-type c$b_5$r. The A and P variants exhibited slightly lowered $T_{50}$ values at 53 and 52 °C, respectively, while the V mutation caused an increase in the value to 57 °C, suggesting a potential small increase in stability. These results suggested that substitution of G179 with alanine, proline, threonine, or valine residues had only modest effects on the thermal stability of the different c$b_5$r variants.

*Enzyme Activities.* Initial-rate kinetic analyses were performed on all four c$b_5$r G179 mutants to evaluate the effects of the various residue substitutions on NAD(P)H utilization. Values derived for $k_{cat}$ and $K_m$ for both NADH:FR and NADPH:FR activities of the various mutants are given in Table 2, together with the corresponding values obtained for wild-type c$b_5$r.

With the exception of the G179A variant, which retained 70% of the wild-type activity with a corresponding 4-fold decrease in affinity for NADH, the remaining three variants exhibited both substantially decreased NADH:FR activities and NADH affinities, with the G179V variant showing the most dramatic changes. NADH catalytic efficiencies, as indicated by $k_{cat}/K_m^{NADH}$, were observed to decrease in the order WT > G179A > G179P > G179T > G179V, with the G179V variant retaining only 0.01% of the NADH:FR efficiency of the wild-type protein. In contrast, NADPH:FR efficiencies, as indicated by the values of $k_{cat}/K_m^{NADPH}$, were only modestly altered and increased in the order G179P < G179V < G179T < WT < G179A, with the G179A mutant exhibiting the smallest increase in NADPH:FR efficiency, corresponding to approximately 8%, when compared to the wild-type protein. It should be noted that, while none of the G179 variants displayed the desired properties of rapid

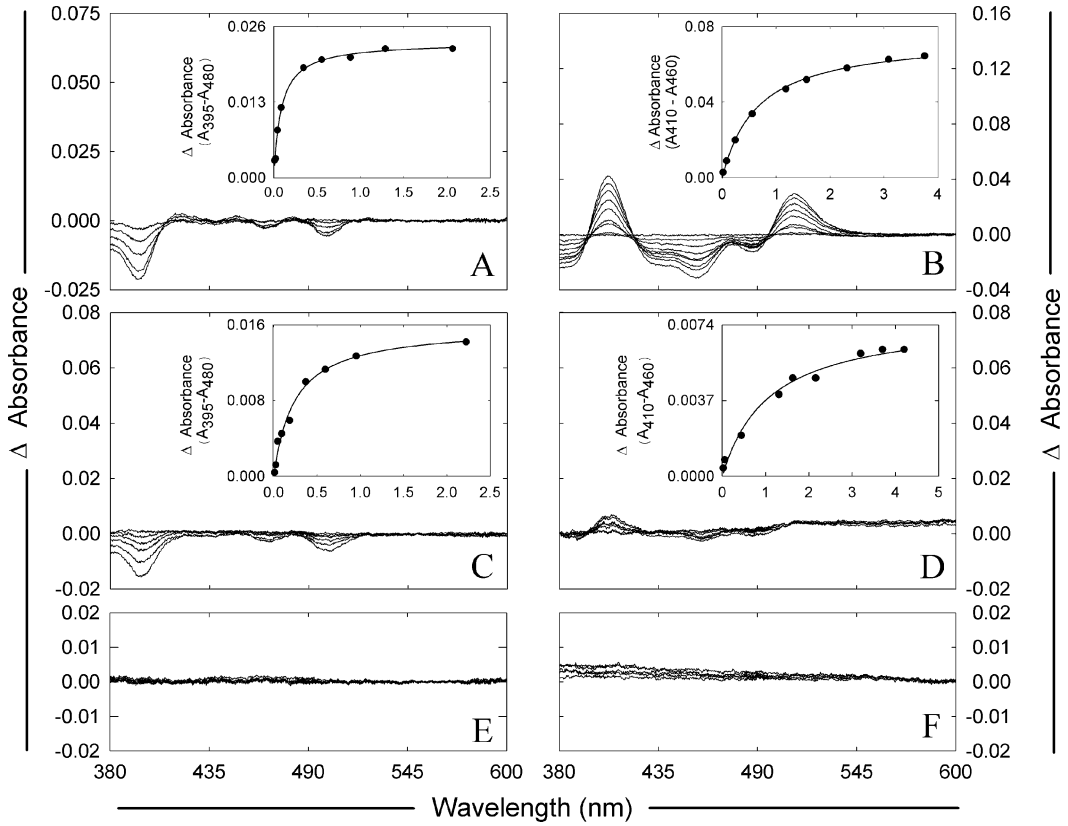


FIGURE 3: Flavin difference spectra obtained following binding of different pyridine nucleotides to wild-type c$b_5$r or the various G179 mutants. Difference spectra were obtained for both wild-type c$b_5$r and the selected G179 mutants at equivalent flavin concentrations (50 $\mu$M FAD) in 20 mM MOPS buffer, containing 0.1 mM EDTA at pH 7.0, following titrations with either $H_4$NAD (left panels) or $NAD^+$ (right panels) as described in the Experimental Procedures. (A and B) wild-type c$b_5$r, (C and D) G179A, (E and F) G179T, G179P, and G179V gave spectra identical to G179T. The inset panels correspond to plots of the magnitudes of the observed spectral perturbations (peak−trough measurements at the indicated wavelengths) versus the ligand concentration. The corresponding $K_s$ values are given in Table 3.

turnover of NADPH, together with a high Michaelis constant for NADH, the G179V variant exhibited both significantly decreased activity with NADH coupled with a substantial decrease in NADH affinity combined with an increased affinity for NADPH.

However, the values for the NAD(P)H specificity constant (defined as the ratio of $\{k_{cat}/K_m^{NADPH}\}/\{k_{cat}/K_m^{NADH}\}$) listed in Table 2 and that reflect the magnitudes of the individual $k_{cat}$ and $K_m$ values obtained for both NADH and NADPH were observed to increase in the order WT < G179A < G179P < G179T < G179V. As anticipated, the relatively conservative substitution of G179 with alanine had the lowest impact on altering the degree of NAD(P)H selectivity, corresponding to only an approximately 7-fold increase in NADPH selectivity. This can be contrasted with increases of 304- and 462-fold for the G179P and G179T variants, respectively, whereas the greatest increase in NADPH selectivity, corresponding to 7692-fold enhancement, was observed for the G179V mutant.

*Differential Spectroscopy.* To compare the interactions of the various G179 variants and wild-type c$b_5$r with various pyridine nucleotides, differential spectroscopy was utilized to monitor complex formation. Alterations of the flavin visible absorbance spectrum, shown in Figure 3, were detected for the wild-type enzyme during titrations with $H_4$-NAD and $NAD^+$ but not with $H_4$NADP or $NADP^+$. These tetrahydronicotinamide derivatives do not function as hydride donors when substituted for NADH in either the NADH:FR or NADH:BR c$b_5$r assays but are valuable tools for examining the binding affinity for NADH and NADPH, respectively. Both $H_4$-nucleotides are close isosteric analogues and are assumed to involve the same contacts at the active site as NADH or NADPH but lack the positive charge on the nicotinamide ring that is present on $NAD^+$ and $NADP^+$, respectively. In contrast, for the G179 mutants, spectroscopically detectable complexes were only observed for the G179A variant with $H_4$NAD, yielding a $K_s$ of 238 $\mu$M, which may be compared with the corresponding value of 85 $\mu$M obtained for wild-type c$b_5$r.

These results suggested that pyridine nucleotides containing 2′-phosporyl groups were most readily accommodated by the G179V variant. The fact that the wild-type c$b_5$r

Table 3: Spectroscopic Binding Constants and Oxidation−Reduction Midpoint Potentials for the FAD/$FADH_2$ Couple in the Various G179 Mutants

| | $K_s$ | | $E^{\circ\prime}$ | | | |
|---|---|---|---|---|---|---|
| protein | $H_4$NAD ($\mu$M) | $NAD^+$ ($\mu$M) | −$NAD^+$ (mV) | slope (mV) | +$NAD^+$ (mV) | slope (mV) |
| G179A | 238 ± 33 | 1083 ± 260 | −272 ± 5 | −29 | −208 ± 5 | −28 |
| G179P | ND[a] | ND[a] | −270 ± 5 | −29 | −224 ± 5 | −32 |
| G179T | ND[a] | ND[a] | −271 ± 5 | −29 | −254 ± 5 | −29 |
| G179V | ND[a] | ND[a] | −274 ± 5 | −31 | −262 ± 5 | −33 |
| wild type | 85 ± 1 | 644 ± 34 | −272 ± 5 | −30 | −194 ± 5 | −62 |

[a] ND indicates that the spectroscopic binding constant for the various pyridine nucleotide could not be determined, owing to insufficient spectral change.

showed no detectable complex formation with any of the 2′-phosphorylated nucleotides suggests a significant role for G179 in discriminating between NADH and NADPH.

*Flavin Oxidation−Reduction Midpoint Potentials.* To examine whether substitution of G179 influenced NAD(P)H utilization through modulation of the flavin oxidation−reduction midpoint potential, potentiometric titrations were performed using the dye equilibration method for wild-type c$b_5$r and the different G179 variants in the presence of phenosafranine ($E^{\circ\prime} = -252$ mV) as an indicator. Flavin midpoint potentials ($E^{\circ\prime}$, $n = 2$) were determined for the enzymes alone and in complex with $NAD^+$. The spectra obtained during representative titrations of G179V in the absence of $NAD^+$ are shown in Figure 4A. Qualitative analysis of the individual spectra obtained from the various titrations indicated that the majority of the phenosafranine was reduced prior to FAD reduction for all four G179 variants and wild-type c$b_5$r in the absence of any pyridine nucleotide, suggesting that the flavin midpoint potentials were more negative than that of phenosafranine, for all of the c$b_5$r variants examined. Analysis of the spectra obtained for the G179A and G179P variants and wild-type c$b_5$r in the presence of $NAD^+$ revealed that the majority of the flavin was reduced prior to the dye, suggesting that complex formation significantly perturbed the flavin midpoint potentials to values more positive than that for phenosafranine for these three proteins. In contrast, the presence of $NAD^+$ had less effect on the titration behavior of the G179T and G179V variants, suggesting little perturbation or modulation of the FAD redox potential.

The flavin redox potentials ($n = 2$) for the different G179 variants and wild-type c$b_5$r alone or as the enzyme−nucleotide complex were determined from the Nernst semilog plots shown in parts B and C of Figure 4. The standard midpoint potentials obtained for the FAD/$FADH_2$ couple in both the wild-type enzyme ($E^{\circ\prime} = -272$ mV) and the different G179 variants ($E^{\circ\prime} = -270$ to $-274$ mV) were approximately equivalent for all five proteins in the absence of any pyridine nucleotide, with the values spanning a range of only 4 mV. In contrast, significant differences in flavin midpoint potential were observed for the wild-type c$b_5$r and the G179 variants in the presence of $NAD^+$. In the presence of $NAD^+$, the redox potential of the FAD/$FADH_2$ couple in the wild-type enzyme was positively shifted by 78 mV ($E^{\circ\prime} = -193$ mV), which may be compared to the values of $-207$ mV for the G179A variant, $-225$ mV for G179P, $-254$ mV for G179T, and $-263$ mV for G179V, respectively, illustrating that the progressively decreased affinity for $NAD^+$ observed in the G179 variants was reflected in progressively smaller perturbations of the flavin redox potential.

The decreased affinity for $NAD^+$ for the G179 mutants was also reflected in alterations in the slopes of the Nernst plots when compared to the wild-type domain. Values obtained for the G179 mutants varied from $-28$ mV (G179A) to $-33$ mV (G179V), consistent with $n = 2$ reduction processes, while in contrast, the wild-type enzyme in the presence of $NAD^+$ exhibited a slope of $-62$ mV, indicative of a $n = 1$ reduction process. These results are in agreement with previous thermodynamic studies of the porcine enzyme (*36*) that indicated that $NAD^+$ binding resulted in stabilization of the flavin semiquinone intermediate, reflecting a change from a $n = 2$ to a $n = 1$ redox process. In contrast, while $NAD^+$ binding to the G170 variants resulted in limited perturbations of the FAD/$FADH_2$

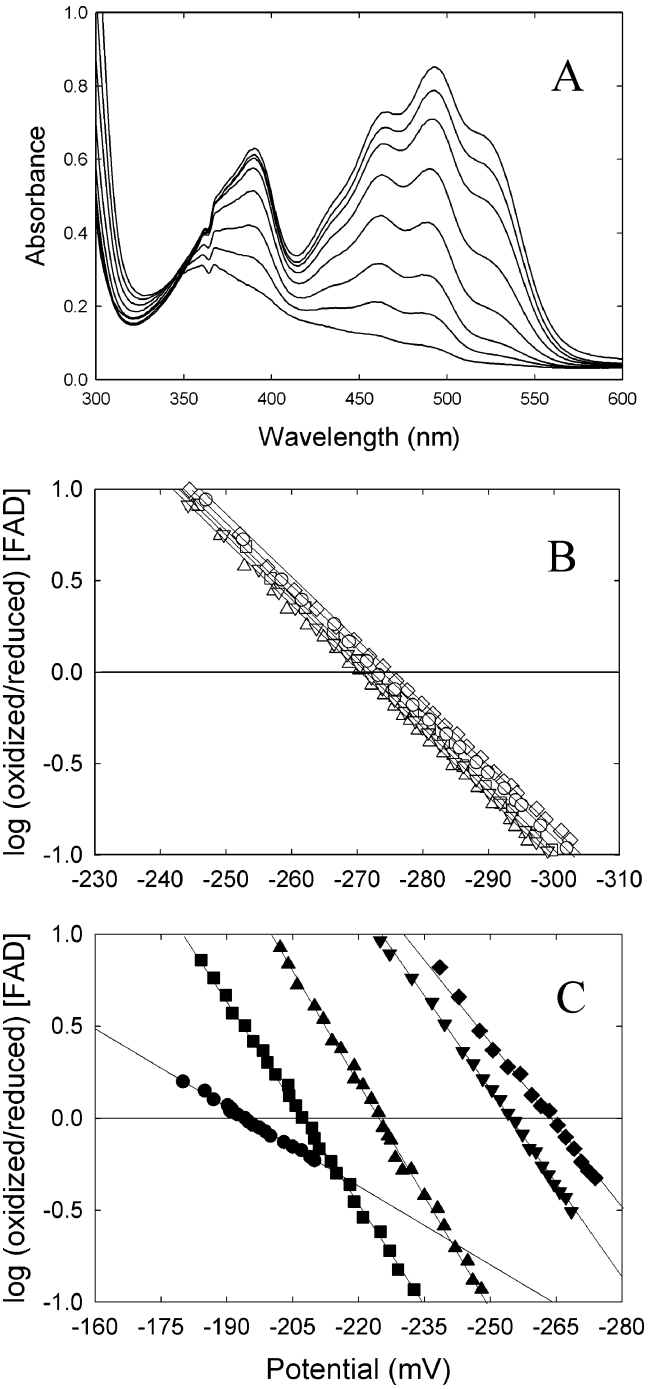


FIGURE 4: Oxidation−reduction midpoint potentials for the FAD prosthetic group in c$b_5$r and the G179 variants. Reductive dye equilibration titrations of the wild type and the different G179 variants of c$b_5$r (40 $\mu$M FAD) were performed as described under the Experimental Procedures in 100 mM phosphate buffer, containing 0.1 mM EDTA at pH 7.0 in the presence of phenosafranine (15 $\mu$M, $E^{\circ\prime} = -252$ mV) (20). Individual spectra were collected at 2−3 min intervals during the time course of the titrations. (A) Representative spectra obtained during a titration of G179V are shown (only a limited number of spectra are shown for clarity). (B) Nernst plots obtained for the FAD/$FADH_2$ couple ($n = 2$) are shown for the titrations of the various G179 mutants and correspond to wild-type c$b_5$r (○), G179A (□), G179P (△), G179T (▽), and G179V (◇). (C) Nernst plots obtained for the FAD/$FADH_2$ couple ($n = 2$) in the presence of $NAD^+$ (2 mM) are shown for the titrations of the various G179 mutants and correspond to wild-type c$b_5$r (●), G179A (■), G179P (▲), G179T (▼), and G179V (◆).

redox potential, the absence of any changes in the slope of the Nernst plots suggested that nucleotide binding did not result in any appreciable semiquinone formation.

## DISCUSSION

The preceding results provide the first documented insights into the role of G179 in maintaining both the structure and function of c$b_5$r and contribute additional evidence to support a role for this residue (or its equivalent) in modulating the pyridine nucleotide selectivity within the flavoprotein transhydrogenase superfamily of enzymes.

A multiple alignment of the 50 currently known c$b_5$r primary structures deposited in GenBank revealed that, of the approximately 275 residues that comprise the flavin- and NADH-binding domains together with the intervening "hinge" region, G179 represents 1 of only 13 conserved residues within the c$b_5$r sequences, suggesting a potentially important role in functionality. Of the 13 residues, 4 (Y93, T94, P95, and G124) and 7 (G179, G180, G182, P185, N209, I215, and G274) are distributed throughout the FAD- and NADH-binding lobes, respectively, while 2 (G143 and P144) are present in the connecting "hinge" region. Several of these conserved residues are components of the four sequence motifs that are characteristic of the flavoprotein transhydrogenase family and have been the subject of previous studies that have contributed to our understanding of the roles of individual residues such as Y93 (*32*), T94 (*37*), and P144 (*38*).

To probe the role of G179 in substrate binding, hydride transfer, and NADH/NADPH discrimination, we have substituted the glycine residue with alternate amino acids that are primarily found at the equivalent position in other members of the FNR superfamily. Analysis of 1293 sequences that contain the "NAD binding 1" domain, identified within the Pfam database (PF00175) (*39*), and that contain the conserved "GxGxxP" nucleotide-binding motif revealed that only a limited number of different residues were observed at the position preceding this motif, which corresponded to G179 in c$b_5$r. Proteins containing the "NAD binding 1" domain exhibited a marked preference for residues that were either proline, threonine, or alanine, in addition to the dominant residue, glycine.

The results of our mutagenesis studies revealed that substitution of G179 primarily affected the kinetic properties of the enzyme with no significant adverse effects on the properties of the FAD chromophore. Absorption and CD spectra and FAD/$FADH_2$ redox potentials in the absence of $NAD^+$ for all four G179 variants were comparable to those of wild-type c$b_5$r, as would be anticipated for mutations limited to the NADH-binding lobe. In contrast, the four amino acid substitutions, A, P, T, and V, were observed to adversely impact NADH utilization, both in terms of decreasing $k_{cat}$ and increasing $K_m$, with the magnitude of the perturbations greatest for the P, T, and V substitutions. The changes in NADH affinity were also reflected in the absence of spectral changes observed during the $H_4$NAD and $NAD^+$ titrations and the more modest shifts in the flavin redox potential in the presence of $NAD^+$.

The crystal structure of the c$b_5$r−$NAD^+$ complex (*20*) has revealed that G179 is situated approximately 4−5 Å distant from the nucleotide opposite the pyrophosphate moiety and in a cleft formed by the ribityl and ribose moieties of $NAD^+$. G179 is not involved in any direct contacts with the pyridine nucleotide, suggesting that side-chain substitutions should not adversely impact substrate utilization. However, G179 and G180 comprise part of a tight 180° turn within the polypeptide backbone that is situated at the apex of strand N$\beta$1 within the NADH-binding lobe and that precedes helix N$\alpha$1, which forms part of the "GxGxxP" motif. Strand N$\beta$1 also makes extensive contacts with strand N$\beta$5, which comprises part of the second conserved pyridine nucleotide-binding motif corresponding to residues C273−M278 ("CGxxxM"). This motif contains the active-site cysteine residue considered to be critical for accurately positioning the nicotinamide moiety prior to efficient hydride transfer (*40*). Analysis of the crystal structure indicates that the close packing of side chains in this region effectively precludes accommodation of side chains other than that of glycine and to a limited extent that of alanine, and that substitution by more bulky groups, such as those of P, T, or V, would potentially result in distortion of the backbone configuration in the region of this turn that would be accompanied by displacement of the side chain of C273 with concomitant decreases in both activity and substrate affinity.

While the results of our mutational studies could be adequately described in terms of potential alterations in the positioning of residues comprising the two conserved pyridine nucleotide-binding motifs, the observed changes in NADH/NADPH discrimination were less obvious. Our prior studies of NADH/NADPH discrimination have been limited to evaluating the contributions of D239 and F251 (*23*) toward regulating pyridine nucleotide specificity. Analyses of a series of both single and double mutants revealed that, while F251 contributed modestly to specificity, construction of a D239T variant resulted in an approximately 40 000-fold increase in the efficiency of NADPH versus NADH utilization. In contrast, the results generated by our G179 mutants revealed that the greatest increase in NADPH/NADH discrimination, corresponding to an approximately 8000-fold increase, was achieved for the G179V variant.

Both sequence and structural analyses have indicated that several residues participate in NAD(H)/NADP(H) discrimination within the FNR superfamily. Changes in NAD(P)(H) specificity have been described for other constituents including FNR (*41*), cytochrome P450 reductase (*42*), and assimilatory nitrate reductase (*43*, *44*), with the latter the only example of pyridine nucleotide coenzyme studies that examined both NADH- and NADPH-specific isoforms of the enzyme. For nitrate reductase, mutagenesis of two residues, S920 and R932, in the NADPH-specific isoform, resulted in a $7.3 \times 10^4$-fold change in nucleotide specificity, whereas substitutions of the same residues in the NADH-specific isoform resulted in only a $6.2 \times 10^3$-fold alteration in selectivity. However, these studies of FNR family members have primarily focused on residues that specifically interact with the 2′-phosphoryl group, while additional amino acid residues clearly participate in regulating pyridine nucleotide selectivity.

Sequence alignments of FNR family members indicate that most of the constituents that favor NADP(H) as a substrate primarily contain the sequence "$^{T}P_{V}$GxGxxP", whereas those that utilize NAD(H) retain a glycine prior to the motif. Mutational studies of the residue prior to the "GxGxxP"

motif, corresponding to G179 within c$b_5$r, have previously been limited to analyses of T155 in *Anabaena* PCC7119 ferredoxin:$NADP^+$ reductase (*25*). In FNR, the hydroxyl group of T155 has been suggested to function in $NADP^+$/$NAD^+$ selectivity by participating in a hydrogen-bond network that is involved in maintaining the correct backbone architecture of a loop comprising residues 261−268 (CGLRGMEE) within the nucleotide-binding lobe that is required for correctly orienting the bound $NADP^+$ for hydride transfer. Generation of the T155G variant revealed displacement of this loop together with an increased affinity for $NAD^+$ and decreased affinity for $NADP^+$. Within c$b_5$r and other NAD(H)-utilizing FNR variants, an alternate arrangement of the hydrogen-bond network is observed, together with a hairpin-like loop structure, corresponding to residues 272−280 (CGPPPMIQ), rich in proline residues. The organization of this proline-rich region would be disrupted by T, P, or V substitutions at G179, resulting in NADH binding in an altered conformation that both decreased NADH activity and affinity, whereas the catalytic efficiency with NADPH would potentially remain unchanged. The current work complements the studies of *Anabaena* FNR and illustrates that mutating the residue preceding the "GxGxxP" motif can alter pyridine nucleotide specificity in favor of either NAD(H) or NADP(H) with varying degrees of efficiency.

Finally, it should be noted that our efforts to alter the NADH/NADPH specificity of c$b_5$r have not generated changes of the magnitude produced for some other dehydrogenases, such as *S. cerevisiae* format dehydrogenase, where construction of the D196A/Y197R double mutant resulted in a 2 500 000-fold change in $NAD^+$/$NADP^+$ specificity (*45*). However, it is clear that, for c$b_5$r, residues positioned both at the pyridine nucleotide-binding site, such as D239 (*23*), and some distance away, including G179, can each have a profound impact on NAD(P)H selectivity, suggesting that multiple mutations may be required to effectively reverse the pyridine nucleotide selectivity of the enzyme.

## REFERENCES


1. Strittmatter, P. (1965) Direct hydrogen transfer from reduced pyridine nucleotides to microsomal cytochrome $b_5$ reductase, *J. Biol. Chem. 240*, 4481−4487.
2. Kitao, T., Sugita, Y., Yoneyama, Y., and Hattori, K. (1974) Methemoglobin reductase (cytochrome $b_5$ reductase) deficiency in congenital methemoglobinemia, *Blood 44*, 879−884.
3. Hultquist, D. E., and Passon, P. G. (1971) Catalysis of methemoglobin reduction by erythrocyte cytochrome $b_5$ and cytochrome $b_5$ reductase, *Nat. New Biol. 229*, 252−254.
4. Oshino, N., Imai, Y., and Sato, R. (1971) A function of cytochrome $b_5$ in fatty acid desaturation by rat liver microsomes, *J. Biochem. 69*, 155−167.
5. Reddy, V., Kupfer, D., and Capsi, E. (1977) Mechanism of C-5 double bond introduction in the biosynthesis of cholesterol by rat liver microsomes, *J. Biol. Chem. 252*, 2797−2801.
6. Hildebrant, A., and Estabrook, R. W. (1971) Evidence for the participation of cytochrome $b_5$ in hepatic mixed-function oxidation reactions, *Arch. Biochem. Biophys. 143*, 66−79.
7. Loughran, P. A., Roman, L. J., Miller, R. T., and Masters, B. S. S. (2001) The kinetic and spectral characterization of the *E. coli*-expressed mammalian CYP4A7: Cytochrome $b_5$ effects vary with substrate, *Arch. Biochem. Biophys. 385*, 311−321.
8. Pugh, E. L., and Kates, M. (1977) Direct desaturation of eicosatrienoyl lecithin to arachidonoyl lecithin by rat liver microsomes, *J. Biol. Chem. 252*, 68−73.
9. Sakuradani, E., Kobayashi, M., and Shimizu, S. (1999) Identification of an NADH−cytochrome $b_5$ reductase gene from an arachidonic acid-producing fungus, *Mortierella alpina* 1S-4, by sequencing of the encoding cDNA and heterologous expression in a fungus, *Aspergillus oryzae*, *Appl. Environ. Microbiol. 65*, 3873−3879.
10. Barrell, B., and Rajandream, M. A. (1994) *GenBank* Direct Submission CAA86908.
11. Fukuchi-Mizutani, M., Mizutani, M., Tanaka, Y., Kusumi, T., and Ohta, D. (1999) Microsomal electron transfer in higher plants: Cloning and heterologous expression of NADH−cytochrome $b_5$ reductase from *Arabidopsis*, *Plant Physiol. 119*, 353−362.
12. Kamath, R. S., Fraser, A. G., Dong, Y., Poulin, G., Durbin, R., Gotta, M., Kanapin, A., Le Bot, N., Moreno, S., Sohrmann, M., Welchman, D. P., Zipperlen, P., and Ahringer, J. (2003) Systematic functional analysis of the *Caenorhabditis elegans* genome using RNAi, *Nature 421*, 231−237.
13. Adams, M. D., Celniker, S. E., Gibbs, R. A., Rubin, G. M., and Venter, C. J. (2000) *GenBank* Direct Submission NM_168479.
14. Strausberg, R. (2003) *GenBank* Direct Submission BC045880.
15. Klein, S. L., Strausberg, R. L., Wagner, L., Pontius, J., Clifton, S. W., and Richardson, P. (2002) Genetic and genomic tools for *Xenopus* research: The NIH *Xenopus* initiative, *Dev. Dyn. 225*, 384−391.
16. Boardman, P. E., Bonfield, J. K., Brown, W. R. A., Carder, C., Chalk, S. E., Croning, M. D. R., Davies, R. M., Francis, M. D., Grafham, D. V., Hubbard, S. J., Humphray, S. J., Hunt, P. J., Maddison, M., McLaren, S. R., Niblett, D., Overton, I. M., Rogers, J., Scott, C. E., Taylor, R. G., Tickle, C., and Wilson, S. A. (2004) *GenBank* Direct Submission BX950830.
17. Pietrini, G., Carrera, P., and Borgese, N. (1988) Two transcripts encode rat cytochrome $b_5$ reductase, *Proc. Natl. Acad. Sci. U.S.A. 85*, 7246−7250.
18. Yubisui, T., Naitoh, Y., Zenno, S., Tamura, M., Takeshita, M., and Sakaki, Y. (1987) Molecular cloning of cDNAs of human liver and placenta NADH−cytochrome $b_5$ reductase, *Proc. Natl. Acad. Sci. U.S.A. 84*, 3609−3613.
19. Carlton, J. M., Angiuoli, S. V., Suh, B. B., Kooij, T. W., Pertea, M., Silva, J. C., Ermolaeva, M. D., Allen, J. E., Selengut, J. D., Koo, H. L., Peterson, J. D., Pop, M., Kosack, D. S., Shumway, M. F., Bidwell, S. L., Shallom, S. J., van Aken, S. E., Riedmuller, S. B., Feldblyum, T. V., Cho, J. K., Quackenbush, J., Sedegah, M., Shoaibi, A., Cummings, L. M., Florens, L., Yates, F. R., III, Raine, J. D., Sinden, R. E., Harris, M. A., Cunningham, D. A., Preiser, P. R., Bergman, L. W., Vaidya, A. B., van Lin, L. H., Janse, C. J., Waters, A. P., Smith, H. O., White, O. R., Salzberg, S. L., Venter, J. C., Fraser, C. M., Hoffman, S. L., Gardner, M. J., and Carucci, D. J. (2002) Genome sequence and comparative analysis of the model rodent malaria parasite *Plasmodium yoelii yoelii*, *Nature 419*, 512−519.
20. Bewley, M. C., Marohnic, C. C., and Barber, M. J. (2001) The structure and biochemistry of NADH-dependent cytochrome $b_5$ reductase are now consistent, *Biochemistry 45*, 13574−13582.
21. Correll, C. C., Ludwig, M. L., Bruns, C. M., and Karplus, P. A. (1993) Structural prototypes for an extended family of flavoprotein reductase: Comparison of phthalate dioxygenase reductase with ferredoxin reductase and ferredoxin, *Protein Sci. 2*, 2112−2133.
22. Dym, O., and Eisenberg, D. (2001) Sequence-structure analysis of FAD-containing proteins, *Protein Sci. 10*, 1712−1728.
23. Marohnic, C. C., Bewley, M. C., and Barber, M. J. (2003) Engineering and characterization of a NADPH-utilizing cytochrome $b_5$ reductase, *Biochemistry 42*, 11170−11182.
24. Hahne, K., Haucke, V., Ramage, L., and Schatz, G. (1994) Incomplete arrest in the outer membrane sorts NADH−cytochrome $b_5$ reductase to two different submitochondrial compartments, *Cell 79*, 829−839.
25. Medina, M., Luquita, A., Tejero, J., Hermoso, J., Mayoral, T., Sanz-Aparicio, J., Grever, K., and Gomez-Moreno, C. (2001) Probing the determinants of coenzyme specificity in ferredoxin−$NADP^+$ reductase by site-directed mutagenesis, *J. Biol. Chem. 276*, 11902−11912.
26. Murataliev, M. B., and Feyereisen, R. (2000) Interaction of NADP(H) with oxidized and reduced P450 reductase during catalysis. Studies with nucleotide analogs, *Biochemistry 39*, 5066−5074.
27. Marohnic, C. C., and Barber, M. J. (2001) Arginine 91 is not essential for flavin incorporation in hepatic cytochrome $b_5$ reductase, *Arch. Biochem. Biophys. 389*, 223−233.
28. Laemmli, U. K. (1970) Cleavage of structural proteins during the assembly of the head of bacteriophage T4, *Nature 227*, 680−685.

29. Beck-von Bodman, S. B., Schuler, M. A., Jollie, D. R., and Sligar, S. G. (1986) Synthesis, bacterial expression, and mutagenesis of the gene coding for mammalian cytochrome $b_5$, *Proc. Natl. Acad. Sci. U.S.A. 83*, 9443−9447.
30. Barber, M. J., Desai, S. K., and Marohnic, C. C. (2001) Assimilatory nitrate reductase: Lysine 741 participates in pyridine nucleotide binding via charge complementarity, *Arch. Biochem. Biophys. 394*, 99−110.
31. Massey, V. (1991) A simple method for the determination of redox potentials, in *Flavin and Flavoproteins 1990* (Curti, B., Ronchi, S., and Zanetti, G., Eds.) pp 59−66, de Gruyter, Berlin, Germany.
32. Marohnic, C. C., Crowley, L. J., Davis, C. A., Smith, E. T., and Barber, M. J. (2005) Cytochrome $b_5$ reductase: Role of the *si*-face residues, proline 92 and tyrosine 93, in structure and catalysis, *Biochemistry 44*, 2449−2461.
33. Müller, F. (1991) Free flavins: Syntheses, chemical, and physical properties, in *Chemistry and Biochemistry of Flavoenzymes* (Müller, F., Ed.) Vol. 1, pp 1−60, CRC Press, Boca Raton, FL.
34. Kuchler, B., Abdel-Ghany, A. G., Bross, P., Nandy, A., Rasched, I., and Ghisla, S. (1999) Biochemical characterization of a variant human medium-chain acyl-CoA dehydrogenase with a disease-associated mutation localized in the active site, *Biochem. J. 337*, 225−230.
35. Bewley, M. C., Davis, C. A., Marohnic, C. C., Taormina, D., and Barber, M. J. (2003) The structure of the S127P mutant of cytochrome $b_5$ reductase that causes methemoglobinemia shows the AMP moiety of the flavin occupying the substrate binding site, *Biochemistry 42*, 13145−13151.
36. Iyanagi, T., Watanabe, S., and Anan, K. F. (1984) One-electron oxidation−reduction properties of hepatic NADH-cytochrome $b_5$ reductase, *Biochemistry 23*, 1418−1425.
37. Kimura, S., Kawamura, M., and Iyanagi, T (2003) Role of Thr-(66) in porcine NADH−cytochrome $b_5$ reductase in catalysis and control of the rate-limiting step in electron transfer, *J. Biol. Chem. 278*, 3580−3589.
38. Davis, C. A., Crowley, L. J., and Barber, M. J. (2004) Cytochrome $b_5$ reductase; the roles of the recessive congenital methemoglobinemia mutants P144L, L148P, and R159*, *Arch. Biochem. Biophys. 431*, 233−244.
39. Bateman, A., Coin, L., Durbin, R., Finn, R. D., Hollich, V., Griffiths-Jones, S., Khanna, A., Marshall, M., Moxon, S., Sonnhammer, E. L. L., Studholme, D. J., Yeats, C., and Eddy, S. R. (2004) The Pfam protein families database, *Nucleic Acids Res. 32*, D138−D141.
40. Shirabe, K., Yubisui, T., Nishino, T., and Takeshita, M. (1991) Role of cysteine residues in human NADH−cytochrome $b_5$ reductase studied by site-directed mutagenesis. Cys-273 and Cys-283 are located close to the NADH-binding site but are not catalytically essential, *J. Biol. Chem. 266*, 7531−7536.
41. Hermoso, J. A., Mayoral, T., Faro, M., Gomez-Moreno, C., Sanz-Aparicio, J., and Medina, M. (2002) Mechanisms of coenzyme recognition and binding revealed by crystal structural analysis of ferredoxin−$NADP^+$ reductase complexed with $NADP^+$, *J. Mol. Biol. 319*, 1133−1142.
42. Elmore, C. L., and Porter, T. D. (2002) Modification of the nucleotide cofactor-binding site of cytochrome P-450 reductase to enhance turnover with NADH *in vivo*, *J. Biol. Chem. 277*, 48960−48964.
43. Shiraishi, N., Croy, C., Kaur, J., and Campbell, W. H. (1998) Engineering of pyridine nucleotide specificity of nitrate reductase: Mutagenesis of recombinant cytochrome *b* reductase fragment of *Neurospora crassa* NADPH:Nitrate reductase, *Arch. Biochem. Biophys. 358*, 104−115.
44. Barber, M. J. (2000) Altered pyridine nucleotide specificity of spinach nitrate reductase, *FASEB J. 14*, A1416.
45. Serov, A. E., Popova, A. S., Fedorchuk, V. V., and Tishkov, V. I. (2002) Engineering of coenzyme specificity of formate dehydrogenase from *Saccharomyces cerevisiae*, *Biochem. J. 367*, 841−847.
46. Thompson, J. D., Gibson, T. J., Plewniak, F., Jeanmougin, F., and Higgins, D. G. (1997) The CLUSTAL X windows interface: Flexible strategies for multiple sequence alignment aided by quality analysis tools, *Nucleic Acids Res. 24*, 4876−4882.
47. Crooks, G. E., Hon, G., Chandonia, J. M., and Brenner, S. E. (2004) WebLogo: A sequence logo generator, *Genome Res. 14*, 1188−1190.

BI051165T